

## THE VARIABILITY OF SAGITTARIUS A\* AT CENTIMETER WAVELENGTHS

ROBESON M. HERRNSTEIN<sup>1</sup>, JUN-HUI ZHAO<sup>2</sup>, GEOFFREY C. BOWER<sup>3</sup>, AND W. M. GOSS<sup>4</sup>  
*Accepted for publication in AJ*

## ABSTRACT

We present the results of a 3.3-year project to monitor the flux density of Sagittarius A\* at 2.0, 1.3, and 0.7 cm with the Very Large Array. Between 2000.5 and 2003.0, 119 epochs of data were taken with a mean separation between epochs of eight days. After 2003.0, observations were made roughly once per month for a total of nine additional epochs. Details of the data calibration process are discussed, including corrections for opacity and elevation effects as well as changes in the flux density scales between epochs. The fully calibrated light curves for Sgr A\* at all three wavelengths are presented. Typical errors in the flux density are 6.1%, 6.2%, and 9.2% at 2.0, 1.3, and 0.7 cm, respectively. There is preliminary evidence for a bimodal distribution of flux densities, which may indicate the existence of two distinct states of accretion onto the supermassive black hole. At 1.3 and 0.7 cm, there is a tail in the distribution towards high flux densities. Significant variability is detected at all three wavelengths, with the largest amplitude variations occurring at 0.7 cm. The rms deviation of the flux density of Sgr A\* is 0.13, 0.16, and 0.21 Jy at 2.0, 1.3, and 0.7 cm, respectively. During much of this monitoring campaign, Sgr A\* appeared to be relatively quiescent compared to results from previous campaigns. At no point during the monitoring campaign did the flux density of Sgr A\* more than double its mean value. The mean spectral index of Sgr A\* is  $\alpha = 0.20 \pm 0.01$  (where  $S_\nu \propto \nu^\alpha$ ), with a standard deviation of 0.14. The spectral index appears to depend linearly on the observed flux density at 0.7 cm with a steeper index observed during outbursts. This correlation is consistent with the expectation for outbursts that are self-absorbed at wavelengths of 0.7 cm or longer and inconsistent with the effects of simple models for interstellar scintillation. Much of the variability of Sgr A\*, including possible time lags between flux density changes at the different wavelengths, appears to occur on time scales less than the time resolution of our observations (8 days). Future observations should focus on the evolution of the flux density on these time scales.

*Subject headings:* Galaxy: center — radio continuum: galaxies — accretion — black hole physics

## 1. INTRODUCTION

Observations of stellar proper motions in the central 1'' (0.04 pc) of the Milky Way suggest that a  $4 \times 10^6 M_\odot$  black hole is located at the dynamical center of the Galaxy (Schödel et al. 2002; Ghez et al. 2003b). In the radio, the bright ( $\sim 1$  Jy), compact source called Sagittarius A\* (Sgr A\*) appears to be closely associated with the supermassive black hole (Menten et al. 1997). For over two decades, the radio flux density of Sgr A\* has been known to vary (Brown & Lo 1982), but the cause of this variability remains unclear. The radio variability tends to increase towards shorter wavelengths, and significant fluctuations on roughly weekly time scales are observed at wavelengths of 2 cm and shorter (Zhao et al. 2001). Based on this observed increase in fractional variability towards shorter wavelengths, the variability of Sgr A\* at centimeter wavelengths has been suggested to be intrinsic to the source (Zhao et al. 1992). At millimeter and sub-millimeter wavelengths, the flux density of Sgr A\* is even more variable (Wright & Backer 1993; Tsuboi et al. 1999; Zhao et al. 2003). Changes of up to a factor of four in the flux density have been observed at 1.3 mm using the Sub-Millimeter Array (SMA) (Zhao et al. 2003).

Short-term variability of Sgr A\* has been detected in

X-rays. In 2002, a multi-wavelength campaign was undertaken to simultaneously monitor Sgr A\* at centimeter, millimeter, infra-red, and X-ray wavelengths. Based on 500 kilo-seconds of Chandra observations, Baganoff (2003) finds that flares of a factor of  $\sim 10$  occur roughly once per day. (In this paper, we call events on hour-to-day time scales “flares”, while events on time scales of weeks are referred to as “outbursts”.) The strongest X-ray flare during this observation occurred on 29 May 2002 and showed a factor of 20 increase in the flux of Sgr A\*. To date, three additional large X-ray flares have been observed between June 2000 and October 2003. On 27 October 2000, the flux of Sgr A\* detected by Chandra increased by a factor of 45 during a 10 ksec flare (Baganoff et al. 2001). A factor of 20 increase in the flux of Sgr A\* at 2–10 keV was detected by XMM-Newton during the beginning of a flare on 4 September 2001, but the observations unfortunately did not include the entire event (Goldwurm et al. 2003). More recently, a factor of 160 flare lasting 2.7 ks was detected with XMM-Newton on 3 October 2002 (Porquet et al. 2003).

Recently, Sgr A\* has been detected for the first time at infrared wavelengths. In the infrared, Sgr A\* appears to show both long-term and short-term variability. The

<sup>1</sup> Department of Astronomy, Columbia University, Mail Code 5246, 550 West 120th St., New York, NY 10027, herrnstein@astro.columbia.edu

<sup>2</sup> Harvard-Smithsonian Center for Astrophysics, 60 Garden Street, Cambridge, MA 02138, jzhao@cfa.harvard.edu

<sup>3</sup> 601 Campbell Hall, Radio Astronomy Lab, UC Berkeley, Berkeley, CA 94720, gbower@astron.berkeley.edu

<sup>4</sup> National Radio Astronomy Observatory, P.O. Box 0, Socorro, NM, 87801, mgoss@aoc.nrao.edu

short-term variability occurs on time scales of  $\sim 1$  hr, similar to the time scale of X-ray events (Genzel et al. 2003). The day to week time scale of the long-term infrared variability is more similar to the time scale of radio outbursts (Ghez et al. 2003b).

In order to understand the detailed nature of the variability of Sgr A\* in the radio, Zhao et al. (2001) (hereafter ZBG01) combined Very Large Array<sup>5</sup> (VLA) data from frequent monitoring of Sgr A\* between 1990.1 and 1993.5 (Zhao et al. 1992) with twenty years of additional archival data from 1977 to 1999. At 1.3 cm, the flux density of Sgr A\* typically varied by 30%, and occasional outbursts of 100% were observed. A comparison of the light curves at 20, 6.0, 3.6, 2.0, and 1.3 cm showed that the largest amplitude variations in flux density occurred at the shortest wavelengths (ZBG01).

Using a Maximum Entropy Method (Press et al. 1989) as well as a classic periodogram augmented with CLEAN to search for periodicities, ZBG01 found a periodicity of  $106 \pm 10$  days ( $1.1(\pm 0.1) \times 10^{-7}$  Hz) at 3.6, 2.0, and 1.3 cm. The light curves were consistent with no phase offset between the three wavelengths. The mean profile of the 106 day cycle at 1.3 cm had a broad peak, roughly  $25 \pm 5$  days wide at full width at half maximum (FWHM), indicating that the variability of Sgr A\* is most likely quasi-periodic in nature. Analysis of data presented in ZBG01 was hindered, however, by highly irregular sampling intervals. Observations were only made on a regular basis (with sampling intervals from 1 to 28 days) between 1990.1 and 1991.5, a small fraction of the entire study. Between 1991.5 and 1993.5, the sampling was less frequent with a maximum sampling interval of 120 days. Gaps in the archival data were as large as 1200 days.

Additional evidence for periodic variability on the order of 100 days has been detected at 2 and 3 mm using 46 epochs of data taken between 1996 and 2000 with the Nobeyama Millimeter Array (NMA) (Tsutsumi et al. 2002). When the data are folded with a period of 106 days, the resulting cycle divides roughly equally into a “high” and “low” activity state. During the high activity state, the flux density of Sgr A\* can vary by as much as a factor of three, while Sgr A\* is relatively quiescent in the low activity state.

Evidence for a period of 57 days was suggested by Falcke (1999) based on 11 cm data from the Green Bank Interferometer (GBI). This result suggested that the 106-day periodicity could be a harmonic of a higher frequency periodicity. Due to sparse sampling over much of the 20 yr baseline, the data presented by ZBG01 were not sensitive to periods shorter than  $\sim 50$  days. A new monitoring campaign in which the flux density of Sgr A\* was regularly monitored on weekly time scales was necessary to search for these short periodicities and detect the shape of outbursts and phase offsets between the different wavelengths.

From June 2000 to October 2003, over 170 hours of VLA observing time were used to monitor the flux density of Sgr A\* at 2.0, 1.3, and 0.7 cm. The results of this 3.3-year project are presented in this paper. Section 3 explains in detail the data calibration, including corrections for opac-

ity effects and errors in absolute flux calibration. The fully calibrated flux densities for Sgr A\* at 2.0, 1.3, and 0.7 cm are presented in §4 and are also listed in their entirety in Table 2. The characteristics of the light curve, including the spectral index and time delay between wavelengths, are also discussed.

This paper deals primarily with data calibration and the general characteristics of the light curve and spectrum. Results from the analysis of these data for periodic or quasi-periodic signals will be presented in subsequent papers. Although §4 briefly compares our light curves to those from monitoring campaigns at other wavelengths, detailed comparisons are presented elsewhere. Zhao et al. (2003) compares the radio light curve to preliminary data from the Sub-Millimeter Array. A separate paper also discusses evidence for correlated events in the radio and X-ray and possible implications for accretion models for Sgr A\* (Zhao et al. 2004). Finally, six Very Long Baseline Array (VLBA) observations were made as part of this monitoring campaign. The results from these observations are presented in Bower et al. (2004).

## 2. OBSERVATIONS

Data were collected in the A, B, C, D, and hybrid configurations of the VLA through projects AZ128 (21 June 2000 – 26 September 2000), AZ129 (5 October 2000 – 27 September 2001), AZ136 (02 October 2001 – 04 January 2003), and AZ143 (13 January 2003 – 14 October 2003). From 2000.5 to 2003.0, the flux density of Sgr A\* at 2.0, 1.3, and 0.7 cm was measured roughly once per week (for a total of 119 epochs). Between 2003.0 and 2003.8, nine additional observations were made once per month in order to increase our sensitivity to long-term periodicities. Although a total of 128 observations were made, problems with weather or instrumentation resulted in the occasional loss of data at one or more wavelengths. Successful flux densities were measured for a total of 115 epochs at 2.0 cm, 124 epochs at 1.3 cm, and 121 epochs at 0.7 cm. Sampling intervals in the finely sampled data range from 1 to 26 days with a mean separation of eight days (and a median separation of seven days). Observations after 2003.0 have a mean and median separation of 30 days. The resulting data are sensitive to periods between roughly 15 and 2000 days.

A typical observation lasted a total of 1 to 2 hours. Either 3C286 or 3C48 served as the primary flux calibrator and 1741–312 (J1744–312) and 1817–254 (J1820–254) were used to track the phase during the observations. (B1950 name conventions are used throughout this paper.) Following an observation of the flux calibrator at 3.6 cm to calibrate offsets in the pointing solutions, four minute integrations were made at 2.0, 1.3, and 0.7 cm. The pointing offsets were then recalculated for 1741–312. Because of the close proximity of the sources, these solutions were also applied to Sgr A\* and 1817–254. Observations of Sgr A\* at all three wavelengths were interleaved between observations of a phase calibrator at roughly 15 minute intervals. A total of 5–15 minutes of integration time on Sgr A\* were obtained at each wavelength for each observation.

<sup>5</sup> The National Radio Astronomy Observatory is a facility of the National Science Foundation operated under cooperative agreement by Associated Universities, Inc.

### 3. DATA REDUCTION

Initial calibration of the data was performed using the Astronomical Image Processing System (*AIPS*). Data from antennas and baselines with large rms noise were flagged. At all three wavelengths, the data were corrected for changes in efficiency as a function of elevation using the most recent gain curves for each antenna. Prior to 25 July 2001, the gain curves at 2.0 and 1.3 cm were applied using the NRAO supplied tasks, *FIXUGAIN* and *FIXKGAIN*. At 0.7 cm, gain corrections were applied using an algorithm we developed specifically for this project. The task also allowed us to correct the 0.7 cm data for losses due to high opacity at low elevation. Because opacity effects should be negligible at longer wavelengths, this correction was not applied to the 2.0 and 1.3 cm data. Beginning 25 July 2001, both the opacity and gain corrections were incorporated directly into the *AIPS* task *FILLM*. These corrections are equivalent to our previous method and we subsequently used *FILLM* to apply opacity and gain corrections to all of our data.

Primary flux density calibration was performed using 3C286 (1328+307), except for 11 epochs where observations later than 20:00 LST forced us to use 3C48 (0134+329). When 3C48 was observed, baselines from 0–40 k $\lambda$  were used in the flux density calibration for all three wavelengths. For all other epochs, the flux density calibration was performed using 3C286 and included all baselines longer than 150 k $\lambda$  at 2.0 cm or 185 k $\lambda$  at 1.3 cm. At both wavelengths, solutions were calculated using 30 second integration times. At 0.7 cm, a model image of 3C286 obtained from C. Chandler of NRAO was used in the flux density calibration, thus allowing the inclusion of all baselines. First, a phase-only flux density calibration was performed using a solution interval equal to the integration time (10 seconds). The final calibration included both amplitude and phase with a 30 second solution interval. The flux density scale calculated from 3C286 or 3C48 was applied to 1741–312 and 1817–254. Phase calibrator flux densities and associated errors for the phase calibrators were measured using the *AIPS* task *GETJY*.

The flux density of Sgr A\* was measured in the  $u,v$  domain. In determining the flux density of Sgr A\*, it is important to avoid contributions from the extended source, Sgr A West, that surrounds the supermassive black hole. In Figure 1, a plot of amplitude versus  $u,v$  distance for Sgr A\* shows the contribution from Sgr A West on baselines  $\lesssim 40$  k $\lambda$  at 1.3 cm (angular scales  $\gtrsim 5''$ ). For observations made in the largest configurations of the VLA, only baselines longer than 100 k $\lambda$  (corresponding to a  $2''$  resolution) were used in the flux density calculation. For more compact arrays, it was necessary to decrease the minimum allowed  $u,v$  distance for the longer wavelength data. At 2.0 cm in C Array and 1.3 cm in D Array, the minimum  $u,v$  distance was 60 k $\lambda$ . In D Array, baselines longer than 40 k $\lambda$  were used for 2.0 cm data. Finally, an initial estimate of the uncertainty in the flux density of Sgr A\* was calculated assuming that Sgr A\* has the same fractional error in flux density ( $\frac{\Delta S}{S}$ ) as the phase calibrators.

#### 3.1. Correcting for Systematic Scaling Errors in the Flux Density Calibration

We present 1.3 cm flux densities for 1817–254 and 1741–312 after initial calibration in *AIPS* in Figure 2. Variability in flux density of the two calibrators is due to a long-term drift in flux density, short-term variability intrinsic to the source, and slight differences in the absolute flux density scale between epochs. In the following paragraphs, we present the method used to calculate and correct for systematic changes in the flux density scale between epochs. Because the intrinsic short-term variability of the calibrators is not known, we assume that calibrators have only long-term drifts in flux density. Short-term variability, which is highly correlated between the two calibrators, is assumed to result from changes in the flux density scale between epochs. These scale factors are quantified and removed from the data. If any intrinsic, short-term variability of the calibrators exists, it is accounted for in the calculation of the final uncertainties in these scale factors presented at the end of this section.

##### 3.1.1. Calculation of Gain Adjustment Factors

To estimate the long-term drift in flux density, a cubic fit has been made to the light curve of each calibrator (see Figure 2). The parameters of the best fit model for 1817–254 and 1741–312 at each wavelength are given in Table 1. At all three wavelengths, 1741–312 is consistent with a cubic profile. Calibrator 1817–254, however, shows little long-term change in flux over our entire monitoring campaign. This is reflected by the relatively small values of the linear, quadratic, and cubic terms for this calibrator (see Table 1).

Both phase calibrators show additional short-term variability that is not accounted for by the cubic model. For each epoch, the ratio of the model flux density to the observed flux density is calculated for each calibrator. If we define calibrator 1 as 1817–254 and calibrator 2 as 1741–312, then these ratios are given by

$$g_1 = S_1/S'_1 \quad \text{and} \quad g_2 = S_2/S'_2, \quad (1)$$

where  $S_i$  is the model flux density from the cubic fit and  $S'_i$  is the observed flux density. The uncertainty in  $g_i$  is calculated as the quadrature sum of the uncertainty in the observed flux density and the uncertainty in the model flux density from the cubic fit. Figure 3 shows a plot of  $g_1$  and  $g_2$  for every epoch during the monitoring campaign. Intrinsic short-term variability of the two calibrators should result in uncorrelated values of  $g_1$  and  $g_2$ . Systematic errors in the absolute flux density scale, however, will appear as a correlation between the two ratios in Figure 3. The values of  $g_1$  and  $g_2$  are well-correlated, indicating that systematic errors in the absolute flux density calibration are a significant component of the calibrator variability.

We calculate a gain adjustment factor (GAF) as the weighted average of  $g_1$  and  $g_2$ :

$$g = \frac{g_1/\sigma_{g_1}^2 + g_2/\sigma_{g_2}^2}{1/\sigma_{g_1}^2 + 1/\sigma_{g_2}^2}. \quad (2)$$

The gain adjustment factors track the systematic change in the flux density scale with time. The GAF “light curve” at 1.3 cm is shown as the solid line in Figure 3. At all three wavelengths, the average value of the GAF is close to 1, indicating that there is no systematic underestimate or overestimate of the flux densities. However, the typical size of the fractional correction increases towards shorter

wavelengths. The standard deviation of  $g$  is 0.07, 0.11, and 0.17 at 2.0, 1.3, and 0.7 cm, respectively.

### 3.1.2. Estimation of Uncertainties

Typical errors in flux density reported by *AIPS* range from 1–3%. The fact that the values of  $g_1$  and  $g_2$  are not identical to within these errors (see e.g. day 486–515 in Figure 3) indicates that *AIPS* has underestimated the true uncertainties in the flux density measurements and/or there is significant intrinsic variability of one or both of the phase calibrators. The errors reported by *AIPS* are statistical and do not include contributions from systematic errors. Due to these systematic errors (e.g. pointing errors) the flux density calibration at any given epoch is expected to be accurate to only 5–10%. The intrinsic variability of the two phase calibrators is not known. Therefore, while both an underestimation of the errors by *AIPS* and intrinsic source variability probably contribute to the difference between  $g_1$  and  $g_2$ , we take the conservative approach and assume that all of the residual variability observed is due to systematic errors in the calibration.

Assuming that the phase calibrators have only slow drifts in flux density and no short-term variability to within the noise, the difference between  $g_1$  and  $g_2$  in Figure 3 can be used to estimate the true rms noise,  $\sigma'$ , in the flux density measurements. This assumption is reasonable for both of our calibrators (see Figure 4). An additional error, calculated as some fraction,  $f$ , of the source flux density, is added in quadrature to the initial error reported by *AIPS*. For epoch  $i$ ,

$$\sigma'(i) = \sqrt{(fS_\nu(i))^2 + \sigma_{AIPS}(i)^2}. \quad (3)$$

The value of  $f$  is chosen such that the fit of the GAFs to the residual variability of the two calibrators has a reduced chi-squared of one. The values of  $f$  for our data are 0.059, 0.057, and 0.078 for 2.0, 1.3, and 0.7 cm, respectively. Final errors in the flux density measurements for Sgr A\* are typically 6.1%, 6.2%, and 9.2% for 2.0, 1.3, and 0.7 cm, respectively.

A gain adjustment factor could not be determined for the observation on 16 June 2003. In this case, we calculate the uncertainty in the flux density measurement as the quadrature sum of the mean uncertainty in the fully-calibrated flux densities of Sgr A\* and the mean size of the gain adjustment factors.

### 3.1.3. Final Light Curves

Fully-calibrated flux densities for 1817–254 and 1741–312 are calculated by multiplying the observed flux density by the gain adjustment factor. The resulting light curves at 1.3 cm are shown in Figure 4. After application of the GAF, the flux densities of both phase calibrators show only long-term drifts to within the uncertainties. For each epoch, the final flux density and associated uncertainty for Sgr A\* is calculated in the same way as for the phase calibrators and is equal to  $gS'_*$ .

## 4. RESULTS

Figure 5 shows the radio light curves of Sgr A\* at 2.0, 1.3, and 0.7 cm. The fully calibrated flux densities and associated errors are listed in Table 2 and in the online

version of this article. Table 3 summarizes the characteristics of the variability of Sgr A\* at each wavelength.

Table 4 shows the mean and standard deviation of the flux density of Sgr A\* as a function of the VLA array in which the observations were made. VLA configurations are changed roughly every four months, with slight variations due to subscription and scheduling. The 16-month cycle begins in the largest configuration (A) and moves to progressively smaller configurations, ending in the D configuration. As the antennas are moved to a new configuration, roughly three weeks are spent in a hybrid array, during which the northern arm of the array remains in the previous (more extended) configuration and the eastern and western arms are in the new (more compact) configuration. These hybrid arrays are used primarily for sources at low declinations. At the end of the cycle, roughly three weeks are spent moving the antennas from the D configuration back to the A configuration. Because the scheduling of configuration changes and the time spent in each configuration can vary by as much as 2–3 weeks, we do not expect the changes in configuration to produce periodic signatures in our data. This point will be discussed in more detail when the data are analyzed for periodicities, but we can conclude from Table 4 that no trends in flux density or variability as a function of observing array are apparent.

Figure 6 plots a histogram of the flux densities at each wavelength using a bin size of 0.05 Jy. This bin size is roughly equal to the mean uncertainty in the flux density of Sgr A\* at 2.0 and 1.3 cm. Uncertainties in the distribution are calculated as the square root of the number of points in each bin. At all three wavelengths, there appears to be a tendency towards a bimodal distribution of flux densities. If the bimodal distribution is real, it may reflect two different states of accretion onto the supermassive black hole.

Significant variability in the flux density is observed at all three wavelengths (see Figure 5). The reduced chi-squared of a fit of a constant flux density to the observed light curve was calculated at each wavelength. The reduced chi-squared is equal to 5.7 at 2.0 cm, 6.7 at 1.3 cm, and 3.9 at 0.7 cm. The similar shape of the three light curves indicates that the flux densities at centimeter wavelengths are also highly correlated. Figure 6 shows high flux density tails in the distributions at 1.3 and 0.7 cm. These tails reflect the increased variability towards shorter wavelengths, consistent with the results of Zhao et al. (1992). The largest variability in flux densities was observed at 0.7 cm, where the flux density of Sgr A\* varied from a minimum value of  $0.63 \pm 0.06$  Jy to a maximum value of  $1.86 \pm 0.16$  Jy. The flux density of Sgr A\* has a standard deviation during our monitoring campaign of 0.13, 0.16, and 0.21 Jy at 2.0, 1.3, and 0.7 cm, respectively.

A comparison of our light curves to the regularly sampled data from ZBG01 indicates that Sgr A\* may have been in a relatively quiescent state from 2000.5 to 2003.8. Between 1990.1 and 1991.5, ZBG01 monitored the flux density of Sgr A\* with sampling intervals ranging from 1 to 28 days. These finely sampled data form a small subset of the entire 20-year ZBG01 dataset. During the 1.4 years of regular observations, two outbursts in which the 1.3 cm flux density of Sgr A\* exceeded twice the mean value were

observed. At least three additional outbursts of smaller amplitude were also observed.

Strong outbursts appear to be less frequent in the recent monitoring data. We observed no outbursts in which the flux density of Sgr A\* doubled. Only one outburst at 2.0 cm had an amplitude  $> 50\%$  higher than the mean flux density ( $0.834 \pm 0.005$  Jy). This outburst occurred on 14 October 2003 and had a flux density of  $1.32 \pm 0.08$  Jy. At 1.3 cm, the largest outburst was a  $4.5\sigma$  event on 16 July 2003 (day 1124). On this date, the flux density of Sgr A\* was  $1.64 \pm 0.10$  Jy, 77% higher than the mean value during our monitoring campaign ( $0.926 \pm 0.005$  Jy). At 0.7 cm, we detected two  $4.1\sigma$  outbursts in which the flux density of Sgr A\* was  $\sim 86\%$  higher than the mean value ( $1.001 \pm 0.008$  Jy). An outburst with a flux density of  $1.86 \pm 0.18$  Jy occurred on 3 October 2002 (day 837), followed by a second outburst on 16 July 2003 (day 1124) with a flux density of  $1.87 \pm 0.16$  Jy. Although there are relatively few strong outbursts overall, many of the largest outbursts at all three wavelengths occurred within the past year. This result suggests that Sgr A\* may have become more active beginning in mid 2003.

Initial comparison of the radio light curves with X-ray observations of Sgr A\* indicates that there may be a correlation between strong X-ray flares and increases in the flux density at centimeter wavelengths. The dates of the four strong X-ray flares discussed in §1 are marked by arrows in Figure 5. In particular, VLA observations made on 03 October 2003, just 13.5 hours after the onset of the factor of 160 flare, show highly elevated flux densities at all three wavelengths. The 0.7 cm flux density for this date ( $1.86 \pm 0.18$  Jy) was one of the two largest flux densities measured during our entire campaign. This date also marked the steepest measured spectral index ( $0.70 \pm 0.10$ , see §4.1). Correlated X-ray and radio variability may provide clues to the underlying physical processes near the supermassive black hole. Comparison of the radio and X-ray light curves, including a discussion of the relationship between the radio and X-ray events on 03 October 2003, is presented in detail in Zhao et al. (2004).

Recent observations of Sgr A\* with the Sub-Millimeter Array (SMA) indicate that sub-millimeter and centimeter flux densities are also correlated. The SMA (operated jointly by the Smithsonian Astrophysical Observatory and the Academia Sinica Institute for Astronomy and Astrophysics) is the first interferometric array to work full-time at wavelengths  $\lesssim 1$  mm. The high resolution of this interferometer will allow Sgr A\* to be separated from the surrounding thermal dust emission from Sgr A West. Although still under construction at the time, monitoring of the flux density of Sgr A\* at 1.3 mm began in 2001 (Zhao et al. 2003). Between March 2001 and July 2002, the flux density of Sgr A\* was measured at 24 epochs with a resolution of  $2-10''$ . The sampling of this dataset is too sparse to search for periodicities or determine the overall characteristics of the light curve, but a comparison with the VLA monitoring data indicates that the brightest flux densities at 1.3 mm occurred at times when the flux densities at centimeter wavelengths were also high (Zhao et al. 2003, see Figure 2). In the future, more frequent SMA observations of Sgr A\* at 1.3 and 0.87 mm will enable a comparison of the light curves at millimeter and centimeter wavelengths

in more detail.

Finally, it has also been suggested that there may be a correlation between the radio flux density of Sgr A\* and the closest approaches of orbiting stars. Loeb (2004) has predicted that the flux density of Sgr A\* will vary on time scales  $> 1$  month due to fluctuations in the mass accretion rate as stars approach and recede from Sgr A\*. The predicted magnitude of an outburst as well as the time delay between closest approach and the outburst are highly uncertain. Ghez et al. (2003a) have identified three periape dates for massive stars in the Galactic Center: SO-19 (1995.639), SO-16 (2000.243) and SO-2 (2002.335). Only the periape for SO-2 occurred during our monitoring campaign (near day 685). We see no evidence in the light curves for an outburst occurring within 100 days of the SO-2 periape. There is also no evidence for an increase in the mean flux density or a change in the spectral index on this time scale. Therefore, we conclude that the emission from Sgr A\* at centimeter wavelengths is not significantly affected on time-scales  $\gtrsim 1$  week by the close approach of massive stars.

#### 4.1. Spectral Index - Flux Density Correlation

The spectral index  $\alpha$  (defined as  $S_\nu \propto \nu^\alpha$ ) can be calculated from the measured flux densities at 2.0, 1.3, and 0.7 cm. In Figure 7, we plot the calculated spectral index at every epoch in which the flux density was determined at all three wavelengths. The calculated values for  $\alpha$  are also listed in Table 2. During the monitoring campaign, the spectral index was observed to vary between  $-0.07 \pm 0.12$  and  $0.70 \pm 0.10$ . The standard deviation of the calculated spectral indices is 0.14. In Figure 8, the spectral index is plotted as a function of the observed flux density at 0.7 cm ( $S_{0.7}$ ). The spectral index depends linearly on  $S_{0.7}$ , with a best fit of  $\alpha = -0.41(\pm 0.04) + 0.57(\pm 0.04)S_{0.7}$ . The tendency towards steeper spectral index during outburst states is consistent with recent observations in the sub-millimeter (Zhao et al. 2003).

Increased fractional variability towards shorter centimeter wavelengths has been used to suggest that the observed variability of Sgr A\* is intrinsic to the source (Zhao et al. 1992). The linear dependence of spectral index on 0.7 cm flux density strongly favors a model in which the observed variability is intrinsic to Sgr A\* and not the result of interstellar scattering. If the flux density variability is caused by an outburst with a self-absorbed synchrotron spectrum (with  $\alpha_{\text{sync}} \approx 2$ ), then the flux density and the spectral index will rise together (e.g., Marscher & Gear (1985)). For our data, the peak spectral index will occur when the self-absorption frequency is equal to 43 GHz (0.7 cm). At this point, the flux density at this frequency will also be at a maximum. As the self-absorption frequency moves to lower frequencies, both the spectral index and the 0.7 cm flux density will decrease, producing a correlation between spectral index and flux density. If the optically thin spectral index is  $\ll 0$ , then the spectral index will quickly become negative when the self-absorption frequency moves to lower frequencies. Because the measured spectral indices for Sgr A\* are almost all greater than zero, the optically thin spectral index must be reasonably flat ( $\alpha_{\text{thin}} \gtrsim -0.5$ ).

Although we believe the above interpretation represents the most likely scenario, it is not unique. Due to the

complexity and peculiarity of the Galactic Center scattering screen, interstellar scattering cannot be ruled out as the source of the observed variability. However, a positive correlation between flux density and spectral index is not generally expected for interstellar scintillation. In simple models of interstellar scattering, the modulation index of the flux density decreases with frequency in the strong scattering regime (Rickett 1990). This would lead to an anti-correlation between spectral index and flux density. Furthermore, the time scale for diffractive scintillation for Sgr A\* is  $< 100$  s while the time scale for refractive scintillation is  $3 \times 10^6$  s, assuming relative velocities for the Earth and the scattering medium of  $\sim 100$  km s $^{-1}$  (Rickett 1990). We detect strong variability on a time scale that falls well in between these characteristic times. Refractive scintillation appears to be only relevant for velocities  $> 1000$  km s $^{-1}$ , which would likely be associated with stellar winds in the central parsec or the accretion flow itself. To match the correlation (and the increased variability at millimeter and sub-millimeter wavelengths), the turbulence must increase substantially with decreasing scale size in the scattering medium.

The mean spectral index of Sgr A\* can be calculated using the average flux densities at all three wavelengths (see Table 3). The best fit to the mean spectral index is  $\alpha = 0.20 \pm 0.01$ . There is strong evidence for a break in the spectrum of Sgr A\* resulting in an excess in the flux density observed at 1 mm (Zylka et al. 1992; Serabyn et al. 1997; Falcke et al. 1998; Zhao et al. 2003). Falcke et al. (1998) calculate a spectral index of  $\alpha = 0.17$  at wavelengths longer than 2 cm, but find a spectral index of  $\alpha = 0.3$  at wavelengths of 2 cm and shorter. This measurement is based on a single epoch of data, and it is not unexpected given the observed standard deviation of the spectral index of 0.14 during our monitoring campaign. Large changes in the spectral index of Sgr A\* can be seen in our data, and many epochs have spectral indices  $\geq 0.3$  (see Table 2). Our data, however, suggest that, on average, the break occurs at wavelengths shorter than 7 mm. Zhao et al. (2003) also find a spectral index of  $0.1 \pm 0.1$  between 2.0 cm and 3 mm using one epoch of VLA data at 2.0, 1.3, and 0.7 cm and a measurement of the flux density at 3 mm made by Tsutsumi et al. (2002). Between 3 mm and 0.87 mm, the spectral index rises to 0.25, indicating that the break in the spectrum occurs near 3 mm. It appears that, like the spectral index, the wavelength of the break in the spectrum is likely variable. Coordinated observations from centimeter to sub-millimeter wavelengths will be necessary to determine the precise characteristics of the break in the spectrum of Sgr A\*.

A prolonged period of increased spectral index and 0.7 cm flux density appeared to begin around 1 September 2002 and has persisted throughout the remainder of the monitoring campaign. This period also corresponds to the time of an observed increase in variability of Sgr A\* (see §4). Before 1 September 2002 (day 805), the weighted mean spectral index was  $0.16 \pm 0.01$  with a standard deviation of 0.11. The mean flux density at 0.7 cm was  $0.94 \pm 0.01$  Jy. After 1 September, the weighted mean of the spectral index and flux density at 0.7 cm increased to  $0.33 \pm 0.02$  and  $1.20 \pm 0.02$  Jy, respectively. The spectral index is also more variable during this time and has a

standard deviation of 0.14.

#### 4.2. Time Delay

The time sampling of our monitoring campaign makes our data sensitive to delays between wavelengths roughly greater than one week. The time delay between the flux density at the three different frequencies is estimated using the non-parametric method of Pelt et al. (1994). This method is used to calculate the dispersion between two irregularly sampled light curves by searching for a magnification and a shift in time of the two curves. The dispersion is essentially the mean square difference between the flux density at two frequencies on a given time scale. Figure 9 shows the dispersion between the light curves for each possible pair of wavelengths. The results strongly favor no delay between any pair of the three frequencies. A minimum is found in the dispersion for delays less than  $\sim 5$  days, which corresponds to the minimum sampling interval in our data. A monitoring campaign with sampling intervals on daily to hourly time scales will be necessary to determine time delays between wavelengths.

We also calculate the auto-dispersion of the data by comparing each light curve with itself. This calculation enables us to estimate the characteristic change in flux density with time. Results for all three wavelengths are similar, and the auto-dispersion for the 0.7 cm light curve is shown in Figure 10. The auto-dispersion grows slowly with time ( $D^2 \propto t^{0.2}$ ). The weak dependence on time is consistent with the fairly static mean flux density that has been observed since the discovery of Sgr A\* (e.g., ZBG01; Bower et al. (2002)).

### 5. CONCLUSIONS

In this paper, we have presented results from a 3.3-year campaign to monitor the flux density of Sgr A\* at centimeter wavelengths using the VLA. The largest amplitude variations are observed at 0.7 cm, consistent with variability increasing towards shorter wavelengths (ZBG01). Overall, however, Sgr A\* appears to be more quiescent than during previous monitoring campaigns. The spectral index of Sgr A\* appears to be strongly correlated with the 0.7 cm flux density. This result strongly favors an emission mechanism in which outbursts are intrinsic to Sgr A\* and are not the result of interstellar scintillation. Regular monitoring of Sgr A\* at the VLA will continue through at least June 2004 with monthly observations at 2.0, 1.3, and 0.7 cm. These additional data will be useful in detecting periods longer than 100 days.

Much of the activity of Sgr A\* appears to take place on time scales  $\gtrsim 1$  hr and less than the time resolution of our data (8 days). However, the monitoring campaigns in the radio and sub-millimeter have only minimally probed these time scales. To date, hourly time scales have only been systematically probed in X-rays and the infrared. In both cases, there is significant variability on time scales of hours. Monitoring of the centimeter flux density on these short time scales will be necessary to determine the duration and shape of outbursts as well as detect any time lag between wavelengths. Additional coordinated multi-wavelength campaigns specifically aimed at probing these time scales should also be implemented. Only with simultaneous coverage and fine sampling will we be able to as-

certain the relationship between radio outbursts and X-ray flares and constrain the emission mechanism for Sgr A\*.

The authors would like to thank C. Fassnacht for help

with the initial data calibration and sharing his code to calculate the dispersion between light curves. We also thank C. Chandler for the model image of 3C286 used in the data calibration and J. Herrnstein for useful discussions.

#### REFERENCES

- Baganoff, F. K. 2003, AAS/High Energy Astrophysics Division, 35  
 Baganoff, F. K. et al. 2001, *Nature*, 413, 45  
 Bower, G. C., Falcke, H., Herrnstein, R. M., Zhao, J.-H., Goss, W. M., & Backer, D. C. 2004, submitted to *Science*  
 Bower, G. C., Falcke, H., Sault, R. J., & Backer, D. C. 2002, *ApJ*, 571, 843  
 Brown, R. L. & Lo, K. Y. 1982, *ApJ*, 253, 108  
 Falcke, H. 1999, in ASP Conf. Ser. 186: The Central Parsecs of the Galaxy, 113  
 Falcke, H., Goss, W. M., Matsuo, H., Teuben, P., Zhao, J., & Zylka, R. 1998, *ApJ*, 499, 731  
 Genzel, R., Schödel, R., Ott, T., Eckart, A., Alexander, T., Lacombe, F. D. R., & Aschenbach, B. 2003, *Nature*, in press  
 Ghez, A. M., Becklin, E., Duchêne, G., Hornstein, S., Morris, M., Salim, S., & Tanner, A. 2003a, in *Astron. Nachr.*, Vol. 324, No. S1, Special Supplement “The central 300 parsecs of the Milky Way”, Eds. A. Cotera, H. Falcke, T. R. Geballe, S. Markoff., Vol. 324, 527–533  
 Ghez, A. M. et al. 2003b, *ApJ*, 586, L127  
 Goldwurm, A., Brion, E., Goldoni, P., Ferrando, P., Daigne, F., Decourchelle, A., Warwick, R. S., & Predehl, P. 2003, *ApJ*, 584, 751  
 Loeb, A. 2004, *MNRAS*, in press (astro-ph/0311512)  
 Marscher, A. P. & Gear, W. K. 1985, *ApJ*, 298, 114  
 Menten, K. M., Reid, M. J., Eckart, A., & Genzel, R. 1997, *ApJ*, 475, L111  
 Porquet, D., Predehl, P., Aschenbach, B., Grosso, N., Goldwurm, A., Goldoni, P., Warwick, R. S., & Decourchelle, A. 2003, *A&A*, 407, L17  
 Press, W. H., Flannery, B. P., Teukolsky, S. A., & Vetterling, W. T. 1989, *Numerical recipes in C. The art of scientific computing* (Cambridge: University Press, 1989)  
 Rickett, B. J. 1990, *ARA&A*, 28, 561  
 Schödel, R. et al. 2002, *Nature*, 419, 694  
 Serabyn, E., Carlstrom, J., Lay, O., Lis, D. C., Hunter, T. R., & Lacy, J. H. 1997, *ApJ*, 490, L77  
 Tsuboi, M., Miyazaki, A., & Tsutsumi, T. 1999, in ASP Conf. Ser. 186: The Central Parsecs of the Galaxy, 105  
 Tsutsumi, T., Miyazaki, A., & Tsuboi, M. 2002, in *American Astronomical Society Meeting 200, #44.09*  
 Wright, M. C. H. & Backer, D. C. 1993, *ApJ*, 417, 560  
 Zhao, J.-H., Bower, G. C., & Goss, W. M. 2001, *ApJ*, 547, L29  
 Zhao, J.-H., Goss, W. M., Lo, K.-Y., & Ekers, R. D. 1992, in ASP Conf. Ser. 31: Relationships Between Active Galactic Nuclei and Starburst Galaxies, 295  
 Zhao, J.-H., Herrnstein, R. M., Bower, G. C., Goss, W. M., & Liu, S. M. 2004, *ApJ*, in press (astro-ph/0401508)  
 Zhao, J.-H., Young, K. H., Herrnstein, R. M., Ho, P. T. P., Tsutsumi, T., Lo, K. Y., Goss, W. M., & Bower, G. C. 2003, *ApJ*, 586, L29  
 Zylka, R., Mezger, P. G., & Lesch, H. 1992, *A&A*, 261, 119

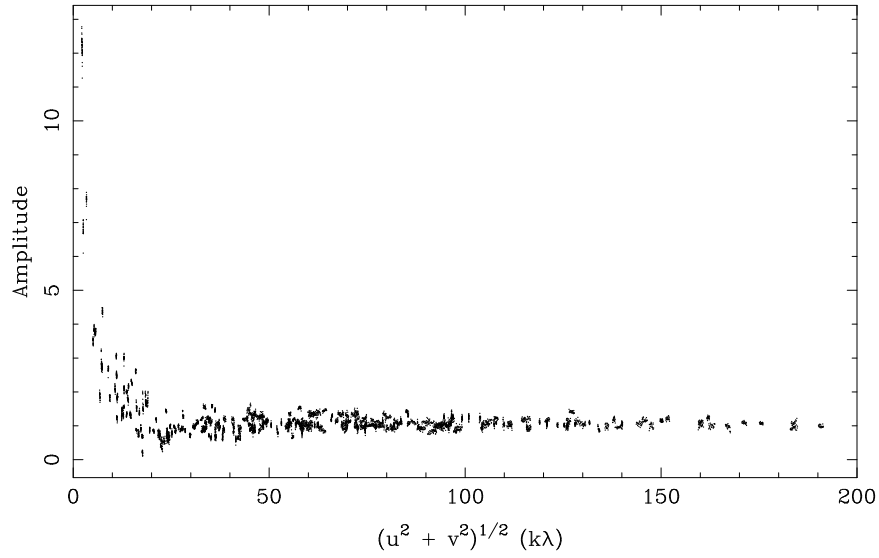


FIG. 1.— Plot of amplitude (in Jy) versus  $u, v$  distance for Sgr A\*. This data was taken at a wavelength of 1.3 cm on 19 December 2002 in the C Array of the VLA. Contributions from Sgr A West are negligible on baselines longer than  $\sim 40 \text{ k}\lambda$ .

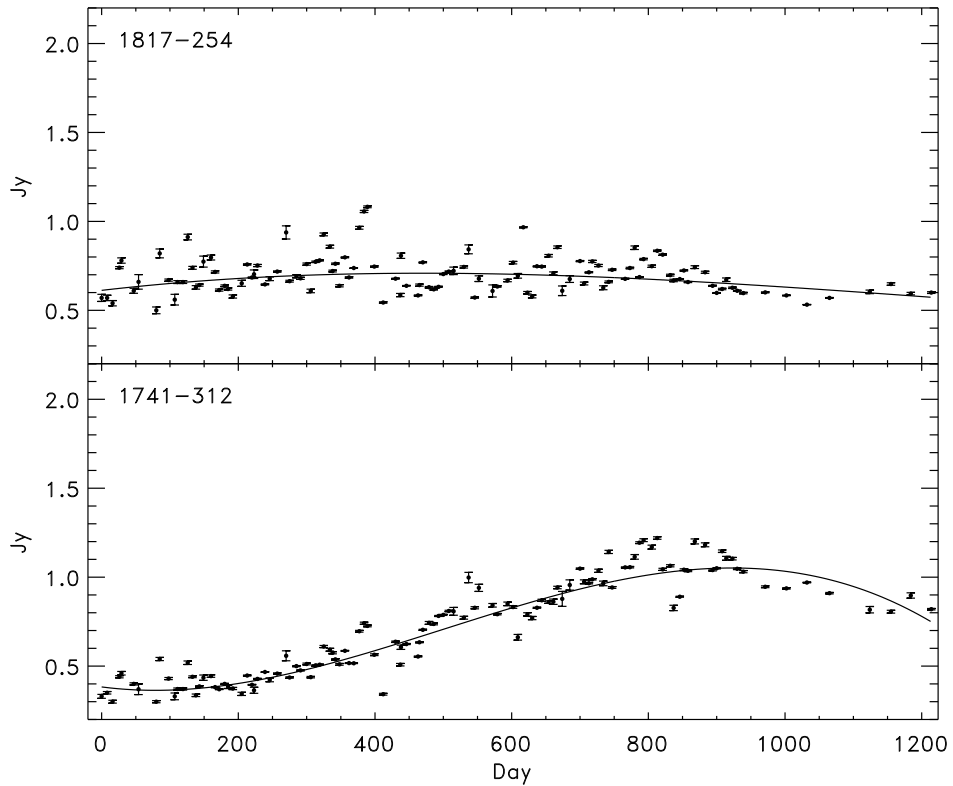


FIG. 2.— Flux density of 1817-254 (*top*) and 1741-312 (*bottom*) at 1.3 cm after calibration in *AIPS*. The best cubic fit to the data is overlaid. The vertical axis is chosen to match Figure 5.



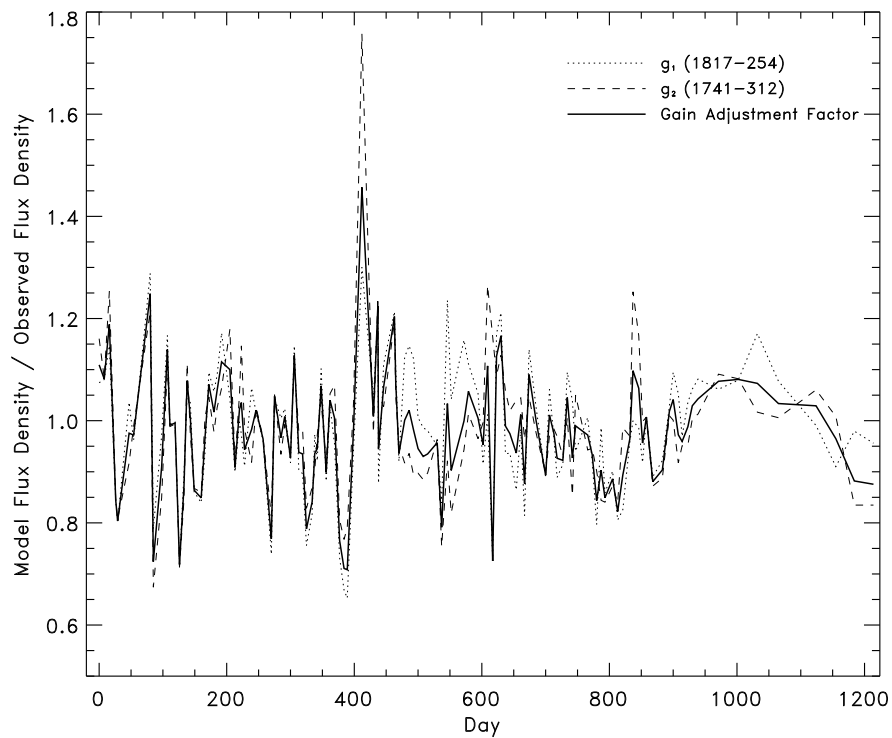


FIG. 3.— Ratio of model flux density derived from the cubic fit to the observed flux density at 1.3 cm for 1817–254 ( $g_1$ ) and 1741–312 ( $g_2$ ). The gain adjustment factor (GAF), calculated as the weighted mean of  $g_1$  and  $g_2$  at each epoch, is overlaid as a solid line (see §3.1.1).

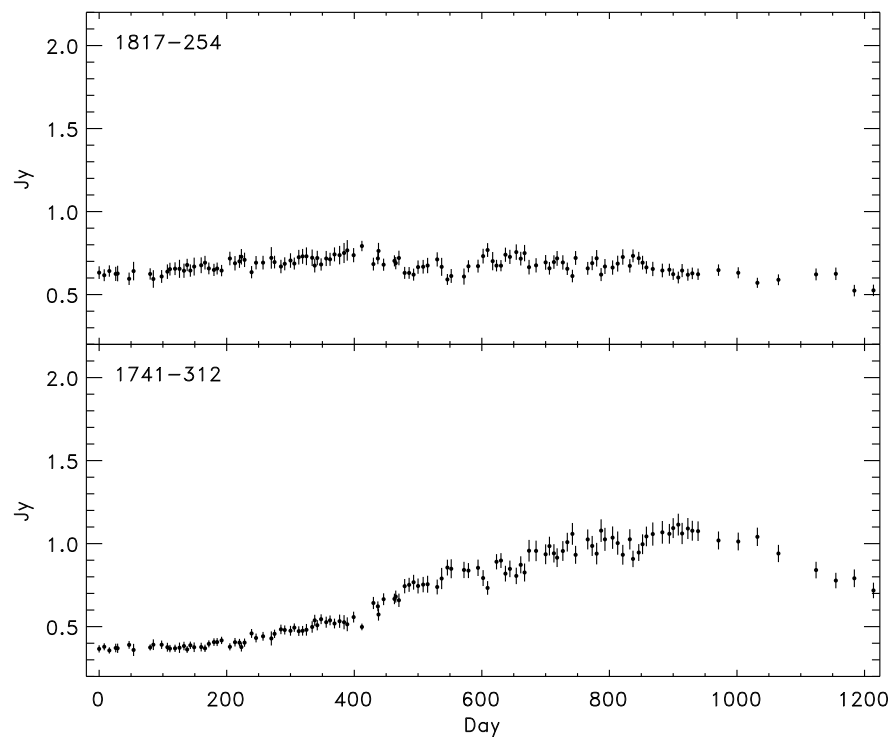


FIG. 4.— Flux density of 1817–254 (*top*) and 1741–312 (*bottom*) at 1.3 cm after application of the gain adjustment factors. Error bars include the original error and the additional fractional error discussed in Section 3.1.2. The vertical axis is chosen to match Figure 5.

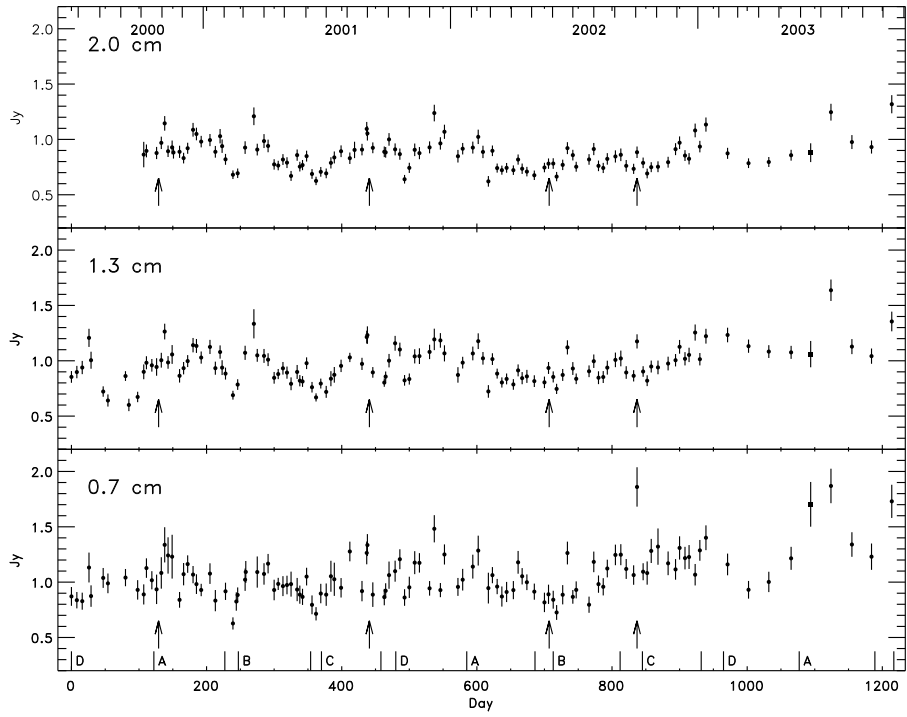


FIG. 5.— Intrinsic variability of Sgr A\* at 2.0, 1.3, and 0.7 cm. The corresponding date is labeled in the top panel and the VLA Array is labeled in the bottom panel. Hybrid configurations are not labeled. Arrows mark four large X-ray flares (see §1).

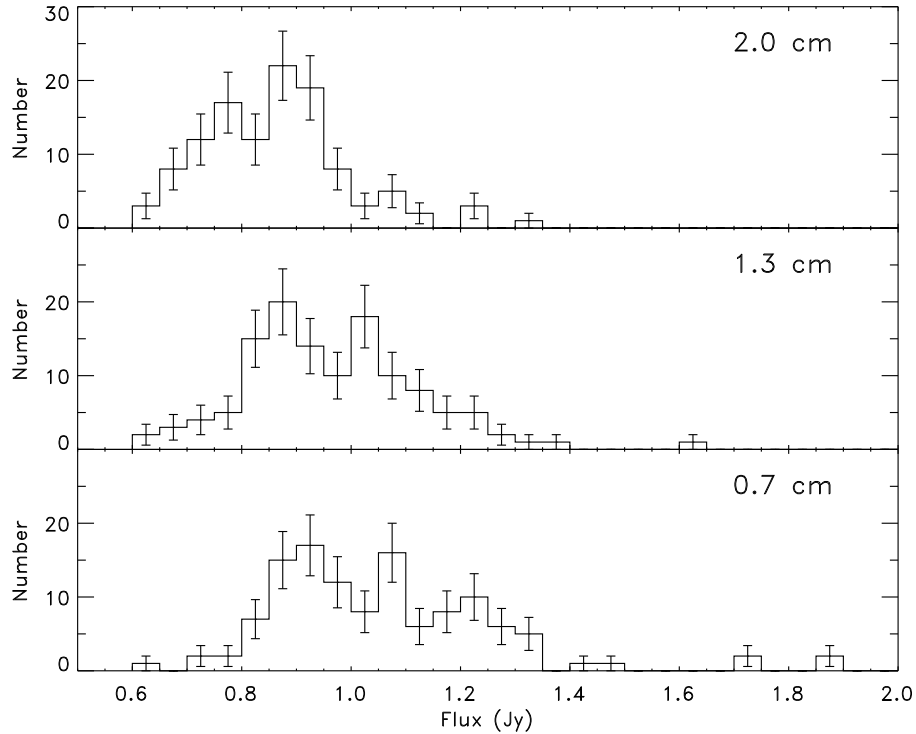


FIG. 6.— Histogram of flux densities at each wavelength. The bin size is 50 mJy. At all three wavelengths, the distribution of flux densities shows evidence for two distinct peaks. A high flux density tail is apparent at 1.3 and 0.7 cm, reflecting the increased variability towards shorter wavelengths.

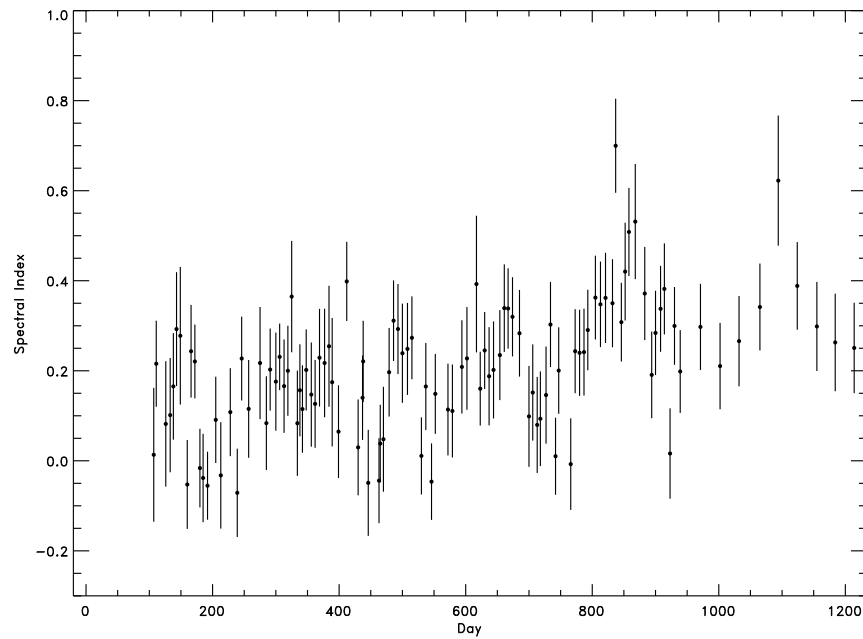


FIG. 7.— Spectral index  $\alpha$  ( $S_\nu \propto \nu^\alpha$ ) as a function of day for every epoch in which flux density measurements were obtained at all three wavelengths.

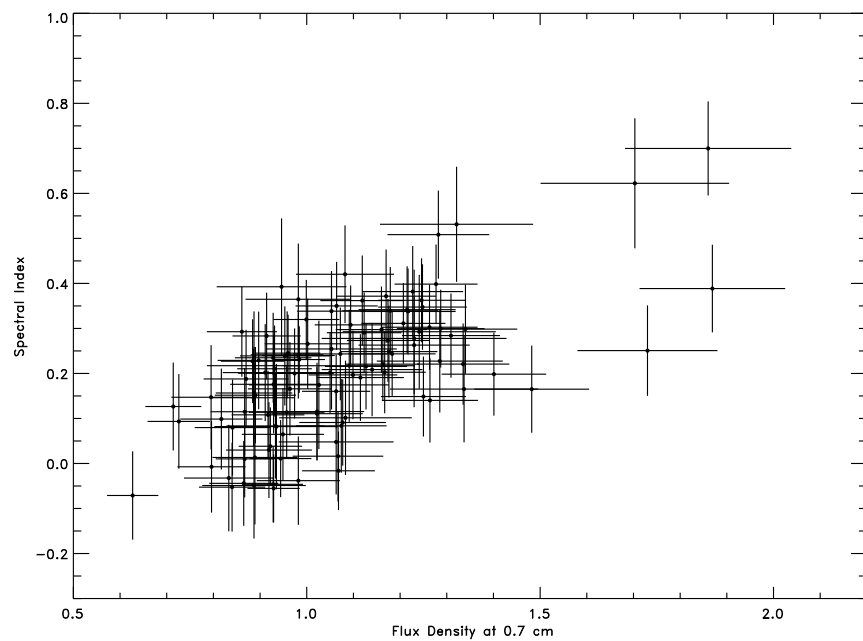


FIG. 8.— Spectral index  $\alpha$  ( $S_\nu \propto \nu^\alpha$ ) as a function of flux density at 0.7 cm. The spectral index becomes steeper during outbursts of Sgr A\*.

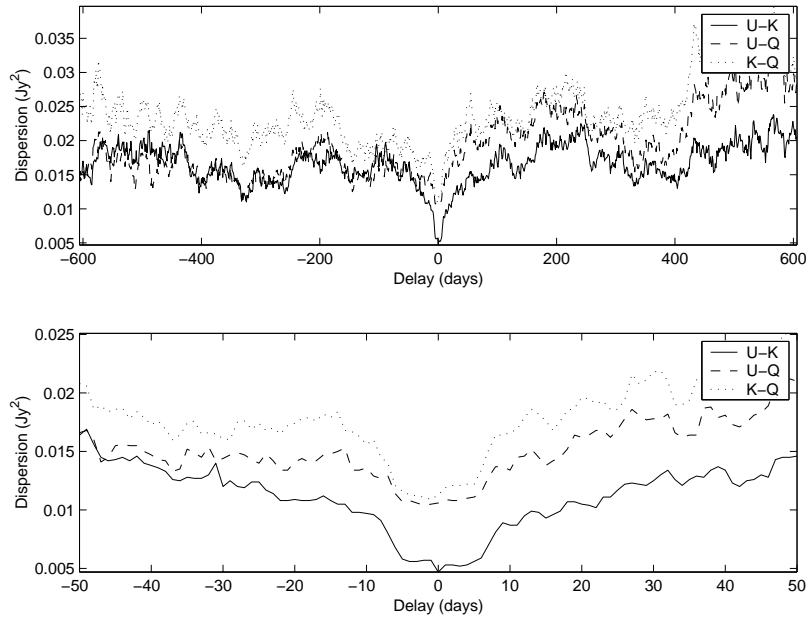


FIG. 9.— The dispersion as a function of time delay between pairs of light curves at the three different frequencies (U=2.0 cm, K=1.3 cm, and Q=0.7 cm). There is a clear minimum in the dispersion at zero delay for each pair.

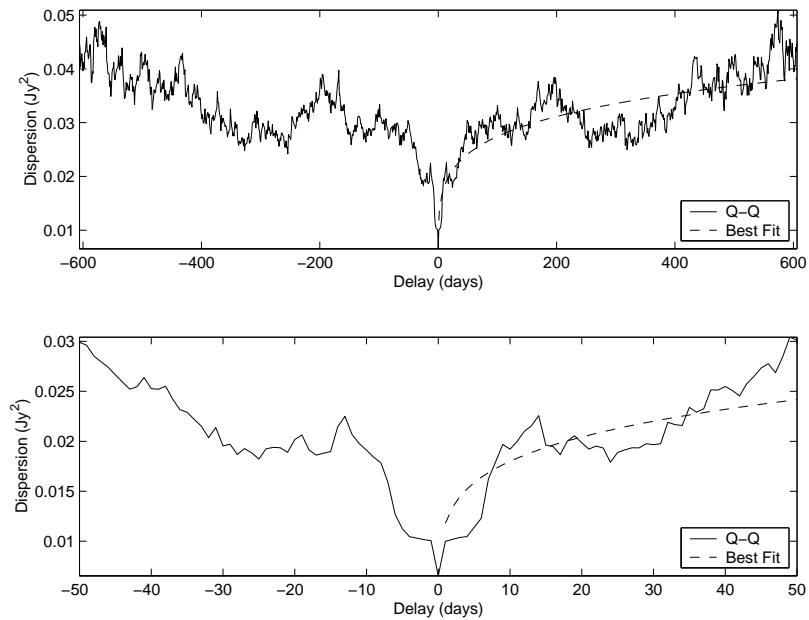


FIG. 10.— The auto-dispersion as a function of time delay for the 0.7 cm light curve. A power-law fit of  $D^2 \propto t^{0.2}$  is also shown.

TABLE 1  
CUBIC FIT PARAMETERS OF PHASE CALIBRATOR

Phase Calibrator	Observing Band	$a_0$ (mJy)	$a_1$ (mJy yr <sup>-1</sup> )	$a_2$ (mJy yr <sup>-2</sup> )	$a_3$ (mJy yr <sup>-3</sup> )
1817–254	2.0 cm	794± 6	47±10	-80±10	17± 8
	1.3 cm	612± 5	162± 8	-78± 6	8± 5
	0.7 cm	388± 5	5± 8	-82± 6	-26± 5
1741–312	2.0 cm	540± 5	-444±10	542± 7	-117± 7
	1.3 cm	383± 5	-182± 9	459± 5	-112± 5
	0.7 cm	287± 6	-163±10	419± 5	-105± 5

Note. — The cubic fit is of the form  $S_\nu = a_0 + a_1x + a_2x^2 + a_3x^3$ , where  $x$  is measured in years and  $x = 0$  corresponds to day 0 in Table 2.

TABLE 2  
CALIBRATED FLUX DENSITY OF SGR A\*

Date	Project day <sup>†</sup>	2.0 cm (Jy)	1.3 cm (Jy)	0.7 cm (Jy)	Spectral Index
20000621	0	...	0.85±0.05	0.87±0.09	...
20000629	8	...	0.90±0.06	0.84±0.07	...
20000707	16	...	0.94±0.06	0.83±0.08	...
20000717	26	...	1.21±0.08	0.13±0.14	...
20000720	29	...	1.00±0.08	0.87±0.10	...
20000806	47	...	0.72±0.05	0.04±0.09	...
20000814	54	...	0.64±0.06	0.99±0.09	...
20000908	80	...	0.86±0.04	0.04±0.08	...
20000913	85	...	0.60±0.06	...	...
20000926	98	...	0.67±0.05	0.93±0.09	...
20001005	107	0.86±0.12	0.90±0.07	0.89±0.09	0.01±0.15
20001009	111	0.90±0.06	0.98±0.06	1.13±0.09	0.22±0.10
20001017	119	...	0.96±0.06	1.02±0.08	...
20001024	126	0.88±0.06	0.94±0.08	0.94±0.13	0.08±0.14
20001031	133	0.97±0.06	1.00±0.07	1.08±0.14	0.10±0.13
20001105	138	1.15±0.07	1.26±0.07	1.34±0.16	0.17±0.12
20001110	143	0.89±0.05	0.99±0.06	1.24±0.16	0.29±0.13
20001116	149	0.93±0.06	1.06±0.09	1.23±0.20	0.28±0.15
20001118	151	0.88±0.06	...	...	...
20001127	160	0.89±0.06	0.86±0.06	0.84±0.07	-0.05±0.10
20001203	166	0.83±0.05	0.93±0.06	1.07±0.10	0.24±0.10
20001209	172	0.92±0.05	1.00±0.05	1.16±0.08	0.22±0.08
20001217	180	1.09±0.06	1.14±0.07	1.07±0.08	-0.02±0.09
20001222	185	1.05±0.06	1.13±0.06	0.98±0.09	-0.04±0.10
20001229	192	0.98±0.05	1.03±0.06	0.93±0.06	-0.06±0.08
20010111	205	0.99±0.06	1.13±0.06	1.08±0.09	0.09±0.10
20010119	213	0.89±0.05	0.93±0.06	0.83±0.10	-0.03±0.12
20010126	220	1.03±0.07	1.08±0.06	...	...
20010129	223	0.94±0.06	0.94±0.07	...	...
20010203	228	0.82±0.05	0.88±0.05	0.92±0.08	0.11±0.10
20010214	239	0.68±0.04	0.69±0.04	0.63±0.06	-0.07±0.10
20010219	244	...	...	0.83±0.08	...
20010221	246	0.69±0.04	0.79±0.05	0.88±0.07	0.23±0.09
20010304	257	0.93±0.06	1.07±0.06	1.02±0.10	0.12±0.11
20010305	258	...	...	1.09±0.10	...
20010317	270	1.21±0.08	1.33±0.13	...	...
20010322	275	0.91±0.05	1.05±0.06	1.09±0.14	0.22±0.12
20010401	285	0.99±0.06	1.04±0.06	1.07±0.10	0.08±0.10
20010407	291	0.94±0.06	1.01±0.06	1.17±0.09	0.20±0.09
20010416	300	0.77±0.05	0.85±0.05	0.93±0.09	0.18±0.11
20010422	306	0.76±0.04	0.88±0.05	0.98±0.06	0.23±0.07
20010429	313	0.82±0.05	0.93±0.06	0.96±0.09	0.17±0.10
20010505	319	0.79±0.05	0.89±0.06	0.97±0.08	0.20±0.10
20010511	325	0.67±0.05	0.79±0.06	0.98±0.11	0.36±0.12
20010520	334	0.86±0.05	0.90±0.06	0.93±0.11	0.08±0.12
20010524	338	0.75±0.04	0.82±0.05	0.89±0.08	0.16±0.10
20010528	342	0.77±0.05	0.81±0.05	0.87±0.07	0.11±0.10
20010603	348	0.85±0.05	0.98±0.05	1.05±0.08	0.20±0.09
20010611	356	0.69±0.04	0.76±0.05	0.80±0.09	0.15±0.12
20010617	362	0.63±0.04	0.67±0.04	0.71±0.06	0.13±0.10
20010624	369	0.71±0.04	0.79±0.05	0.90±0.09	0.23±0.11
20010702	377	0.69±0.04	0.72±0.05	0.89±0.10	0.22±0.12
20010709	384	0.79±0.05	0.84±0.07	1.05±0.14	0.25±0.13
20010714	389	0.84±0.05	0.87±0.07	1.03±0.15	0.17±0.14
20010724	399	0.89±0.05	0.95±0.06	0.95±0.09	0.06±0.10
20010805	412	0.83±0.05	1.03±0.04	1.28±0.09	0.40±0.09
20010813	419	0.91±0.07	...	...	...

TABLE 2—*Continued*

Date	Project day <sup>†</sup>	2.0 cm (Jy)	1.3 cm (Jy)	0.7 cm (Jy)	Spectral Index
20010824	430	0.91±0.05	0.97±0.06	0.92±0.09	0.03±0.11
20010831	437	1.10±0.06	1.21±0.06	1.26±0.10	0.14±0.09
20010901	438	1.05±0.06	1.23±0.08	1.34±0.10	0.22±0.09
20010909	446	0.92±0.05	0.90±0.05	0.89±0.11	-0.05±0.12
20010926	463	0.89±0.05	0.80±0.04	0.87±0.07	-0.04±0.09
20010928	465	0.88±0.05	0.86±0.05	0.92±0.07	0.04±0.09
20011003	470	1.00±0.06	1.00±0.06	1.06±0.12	0.05±0.12
20011011	479	0.91±0.05	1.16±0.07	1.10±0.10	0.20±0.10
20011018	486	0.87±0.05	1.10±0.06	1.21±0.09	0.31±0.09
20011025	493	0.64±0.04	0.82±0.05	0.86±0.08	0.29±0.10
20011101	500	0.74±0.05	0.84±0.05	0.95±0.10	0.24±0.11
20011109	508	0.91±0.06	1.04±0.06	1.18±0.10	0.25±0.10
20011118	515	0.88±0.06	1.04±0.07	1.17±0.09	0.27±0.09
20011201	530	0.93±0.05	1.08±0.07	0.94±0.07	0.01±0.09
20011208	537	1.24±0.08	1.19±0.10	1.48±0.12	0.17±0.10
20011217	546	0.96±0.06	1.18±0.07	0.93±0.06	-0.05±0.08
20011223	552	1.07±0.06	1.07±0.07	1.25±0.09	0.15±0.09
20020112	572	0.85±0.06	0.87±0.07	0.96±0.08	0.11±0.10
20020119	579	0.92±0.05	0.98±0.05	1.02±0.10	0.11±0.10
20020203	594	0.93±0.05	1.07±0.06	1.14±0.11	0.21±0.10
20020211	602	1.02±0.07	1.18±0.07	1.29±0.14	0.23±0.11
20020218	609	0.89±0.06	1.02±0.06	...	...
20020226	617	0.62±0.05	0.72±0.06	0.95±0.14	0.39±0.15
20020304	623	0.90±0.05	1.01±0.05	1.06±0.07	0.16±0.08
20020311	630	0.74±0.04	0.88±0.05	0.96±0.07	0.25±0.09
20020318	637	0.72±0.04	0.80±0.05	0.87±0.09	0.19±0.11
20020325	644	0.74±0.04	0.84±0.05	0.91±0.09	0.20±0.11
20020404	654	0.72±0.04	0.79±0.05	0.93±0.08	0.23±0.10
20020411	661	0.82±0.05	0.91±0.05	1.18±0.10	0.34±0.10
20020417	667	0.74±0.05	0.84±0.06	1.05±0.07	0.34±0.09
20020424	674	0.71±0.04	0.86±0.06	1.00±0.07	0.32±0.09
20020505	685	0.68±0.04	0.82±0.05	0.91±0.07	0.28±0.10
20020520	700	0.75±0.04	0.81±0.05	0.82±0.09	0.10±0.11
20020526	706	0.78±0.05	0.94±0.05	0.89±0.09	0.15±0.11
20020602	713	0.78±0.05	0.85±0.05	0.84±0.08	0.08±0.11
20020607	718	0.66±0.04	0.75±0.05	0.73±0.07	0.09±0.11
20020616	727	0.77±0.05	0.87±0.05	0.89±0.09	0.15±0.11
20020623	734	0.92±0.05	1.12±0.06	1.26±0.10	0.30±0.09
20020701	742	0.86±0.05	0.93±0.06	0.87±0.06	0.01±0.09
20020706	747	0.75±0.05	0.84±0.05	0.93±0.08	0.20±0.10
20020725	766	0.82±0.05	0.91±0.05	0.80±0.07	-0.01±0.10
20020801	773	0.91±0.06	1.00±0.06	1.18±0.09	0.24±0.09
20020808	780	0.76±0.05	0.85±0.06	0.98±0.08	0.24±0.10
20020815	787	0.74±0.05	0.85±0.05	0.96±0.08	0.24±0.10
20020820	793	0.82±0.05	0.94±0.06	1.12±0.08	0.29±0.09
20020901	805	0.85±0.06	1.01±0.07	1.25±0.09	0.36±0.09
20020910	813	0.86±0.06	1.02±0.07	1.25±0.10	0.35±0.09
20020918	821	0.76±0.05	0.89±0.06	1.12±0.09	0.36±0.10
20020928	832	0.73±0.05	0.86±0.05	1.06±0.09	0.35±0.10
20021003	837	0.88±0.05	1.18±0.06	1.86±0.18	0.70±0.10
20021012	846	0.79±0.05	0.90±0.05	1.09±0.08	0.31±0.09
20021018	852	0.69±0.04	0.82±0.05	1.08±0.11	0.42±0.11
20021024	858	0.75±0.05	0.95±0.05	1.28±0.11	0.51±0.10
20021103	868	0.75±0.05	0.94±0.06	1.32±0.16	0.53±0.13
20021118	883	0.79±0.05	0.98±0.06	1.17±0.11	0.37±0.10
20021129	894	0.91±0.05	1.00±0.06	1.12±0.09	0.19±0.10
20021205	900	0.97±0.06	1.13±0.06	1.31±0.11	0.28±0.09

TABLE 2—*Continued*

Date	Project day <sup>†</sup>	2.0 cm (Jy)	1.3 cm (Jy)	0.7 cm (Jy)	Spectral Index
20021213	908	0.85±0.05	1.02±0.06	1.22±0.10	0.34±0.10
20021219	914	0.83±0.05	1.05±0.07	1.23±0.11	0.38±0.10
20021228	923	1.08±0.06	1.25±0.07	1.07±0.10	0.02±0.10
20030104	930	0.94±0.05	1.01±0.06	1.29±0.09	0.30±0.09
20030113	939	1.13±0.06	1.22±0.07	1.40±0.11	0.20±0.09
20030214	971	0.87±0.05	1.23±0.07	1.16±0.10	0.30±0.10
20030317	1002	0.79±0.04	1.13±0.06	0.93±0.08	0.21±0.10
20030416	1032	0.80±0.05	1.08±0.06	1.00±0.09	0.27±0.10
20030519	1065	0.86±0.05	1.08±0.06	1.22±0.10	0.34±0.10
20030616	1094	0.88±0.09	1.06±0.12	1.70±0.20	0.62±0.14
20030716	1124	1.25±0.08	1.64±0.10	1.87±0.16	0.39±0.10
20030816	1155	0.98±0.06	1.13±0.07	1.34±0.11	0.30±0.10
20030914	1184	0.93±0.06	1.04±0.07	1.23±0.12	0.26±0.11
20031014	1214	1.32±0.08	1.36±0.09	1.73±0.15	0.25±0.10

<sup>†</sup>Project day 0 is 21 June 2000. Days refer to LST days such that observations occurred at roughly the same time each day.

TABLE 3  
PARAMETERS FOR THE FLUX DENSITY VARIABILITY OF SGR A\*

Wavelength (cm)	Number of Epochs	$\langle S_\nu \rangle$ (Jy)	$S_{min}$ (Jy)	$S_{max}$ (Jy)	$\sigma$ (Jy)	$\chi_r^2$ of Fit to Constant $S_\nu$
2.0	115	0.834±0.005	0.62±0.05	1.32±0.08	0.13	5.7
1.3	124	0.926±0.005	0.60±0.06	1.64±0.10	0.16	6.7
0.7	121	1.001±0.008	0.63±0.06	1.87±0.16	0.21	3.9

Note. — The error in the mean flux density is calculated as the weighted error from all measurements. The standard deviation of the measured flux densities at each wavelength is given as  $\sigma$ .

TABLE 4  
FLUX DENSITY AS A FUNCTION OF ARRAY

Array	2.0 cm			1.3 cm			0.7 cm		
	Number of Epochs	$\langle S_\nu \rangle$ (Jy)	$\sigma$ (Jy)	Number of Epochs	$\langle S_\nu \rangle$ (Jy)	$\sigma$ (Jy)	Number of Epochs	$\langle S_\nu \rangle$ (Jy)	$\sigma$ (Jy)
A	33	0.86	0.14	32	0.96	0.17	29	1.03	0.24
BnA	6	0.77	0.24	6	0.83	0.23	7	0.83	0.35
B	26	0.81	0.11	26	0.91	0.12	26	0.97	0.13
CnB	7	0.73	0.09	7	0.83	0.17	7	0.95	0.38
C	21	0.85	0.12	20	0.97	0.14	20	1.13	0.15
DnC	5	0.94	0.11	5	0.94	0.18	5	1.01	0.21
D	17	0.85	0.13	28	0.93	0.17	27	1.00	0.16

Note. — The standard deviation is calculated from the spread of measured flux densities for that array. BnA refers to the hybrid array of the VLA with the northern arm in the A configuration (see §4).